nature geoscience

SUPPLEMENTARY INFORMATION

DOI: 10.1038/NGEO1158

Characteristic Slip for 5 great earthquakes along the Fuyun fault in China.

Klinger[1] Y., Etchebes[1] M., Tapponnier[2] P., and Narteau[1] C.

[1] Institut de Physique du Globe de Paris, Sorbonne Paris Cité, Univ. Paris Diderot, UMR 7154 CNRS, 1 rue Jussieu, F-75005 Paris, France.

[2] EOS, NTU, Singapore.

Supplementary Material

Table of content

Separate accompanying supplementary information files:

2/ SuppTable1 is an excel table with the tabulated offset data presented in this study. (ngeo1158-s2)

3/ SuppTable2 is an excel data with the tabulated data of Jiangbang et al. (1984) and Lin et Lin (1998).
(ngeo1158-s3)

Characteristic Slip for 5 great earthquakes along the Fuyun fault in China. Klinger et al.

1/ **Offset measurements from Quickbird satellite images**

Method :

The presence of readily visible offsets at scales of 1/2000 to 1/5000 on the images guided our selection of measurement sites. At each site, the fault trace was mapped and minimal, maximal, and preferred offset values were determined, by realigning each marker (terrace riser, gully channel...) displaced by fault motion. Beyond pixel size, the reconstruction uncertainties depend on marker size and sharpness, orientation relative to the fault trace and width of the fault zone. Each measurement was done manually. Typical apertures used to define piercing lines on either side of the fault were several tens to a hundred meters. The sharpness of the Quickbird images and field inspection of key outcrops (supplementary figure 1b) ensured that mis-identification of either rupture trace or piercing line was kept to a minimum. In this respect, the Fuyun dataset is exceptional because a large number of offset values derived from remote sensing and field measurements can be compared. Depending on the kind of image used, it has been suggested that field measurements tend to provide minimum offset values (Lienkaemper et al., 2001; Klinger et al., 2005, Zielke et al., 2010). In other cases, however, field observations appear to have mislead workers into interpreting cumulative as single event offsets, yielding overestimates of the latter (see discussion in Xu et al., 2006). Here, the relative simplicity and freshness of the rupture trace, as well as the high quality of the images make the correlation between field and satellite data unusually good (see supplementary fig. 1b), even though 1:1 comparisons are not possible because the exact locations of the field values are not published (see supplementary Table 2).

In addition to the actual accuracy attached to each offset measurement, an assessment of robustness is provided (see supplementary Table 1), based on the number of other features this particular offset value realigns in its immediate vicinity along the rupture trace (to distances of ~ 100m on either side). If 10 or more “side” features are thus restored, a maximum robustness index of 5 is attributed to the offset value. If only 2 such additional features are realigned, a robustness index of 1 is appropriate. In fine, the dataset presented in supplementary Table 1 gives for each measurement site a band limited offset range with minimal, maximal, preferred values, and robustness index on a 1 to 5 scale.

Figure 1a: Location of sites D1 to D15 along the 1931 rupture.

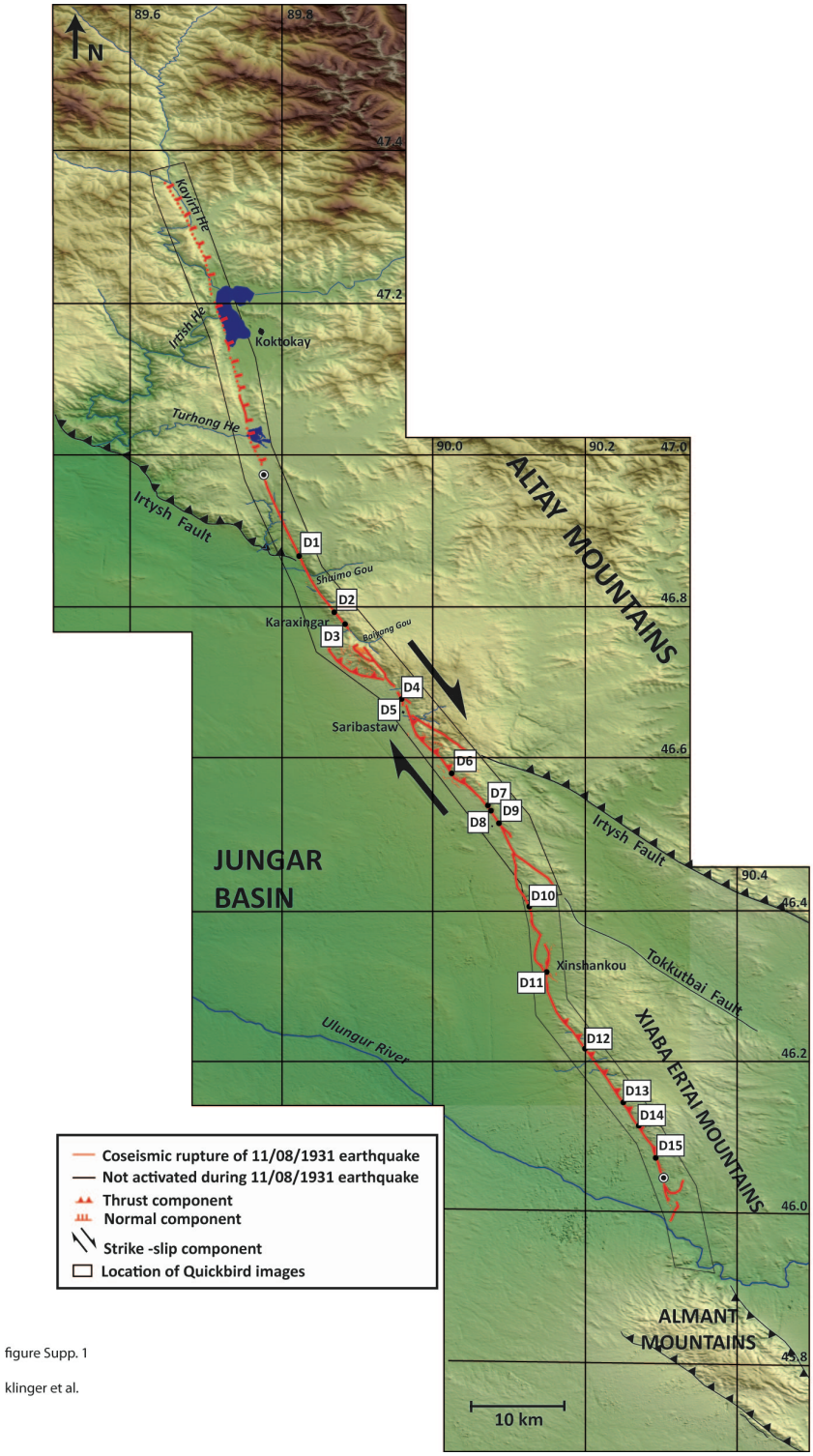

Figure 1b : Example of comparison between field and Quickbird measurements to calibrate the latter

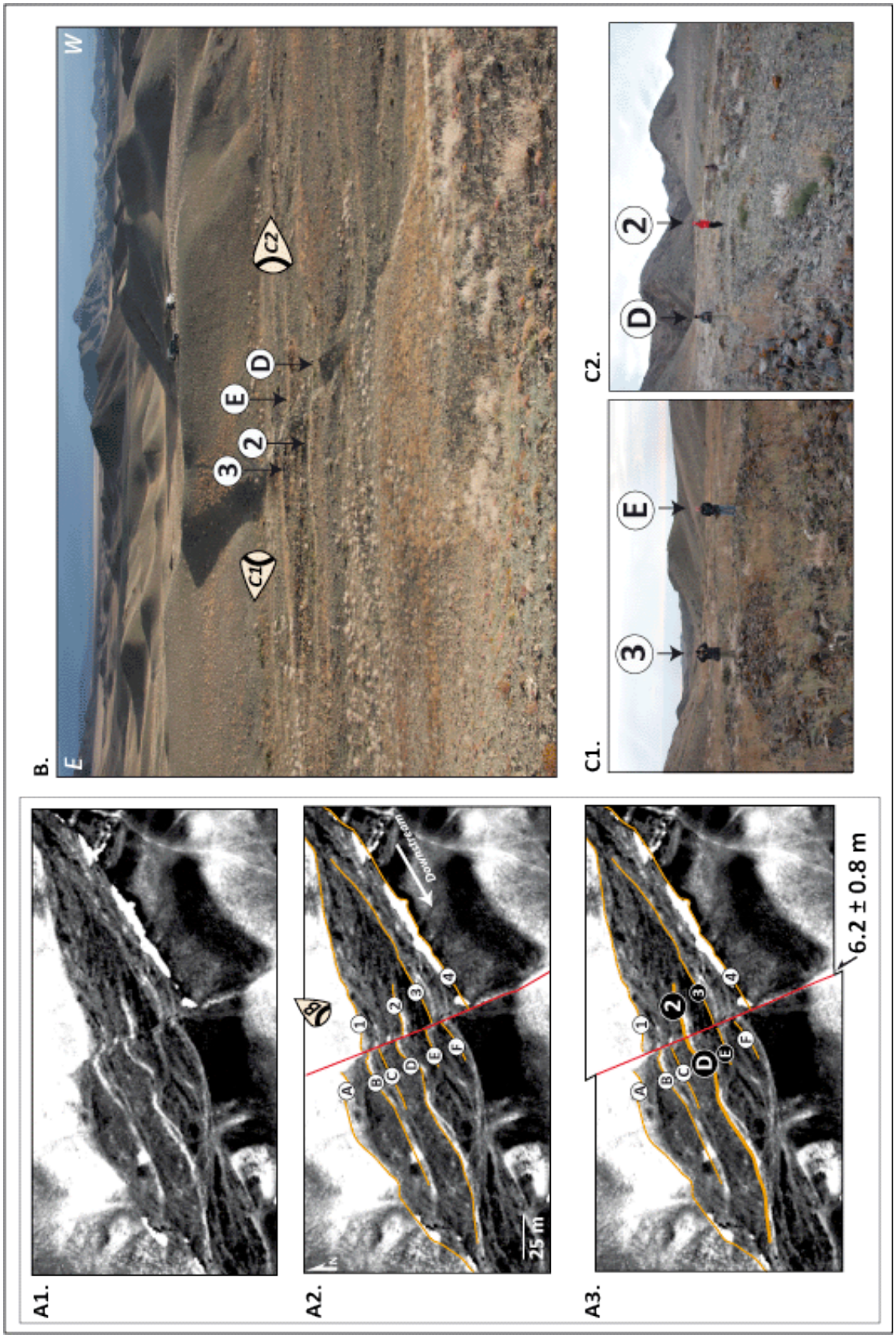

Figures 2a to 2n: Examples of reconstructions of multiple offset measurements at 14 selected sites along rupture (location in fig. 1a). At each site, present-day un-interpreted image is shown next to map of landforms and channels used to determine offsets. Successive restorations are then presented. Circles indicate piercing lines fits that constrain landform restorations (symbols as in main text fig. 2).

Figure Supp. 2a
klinger et al.

SITE D1

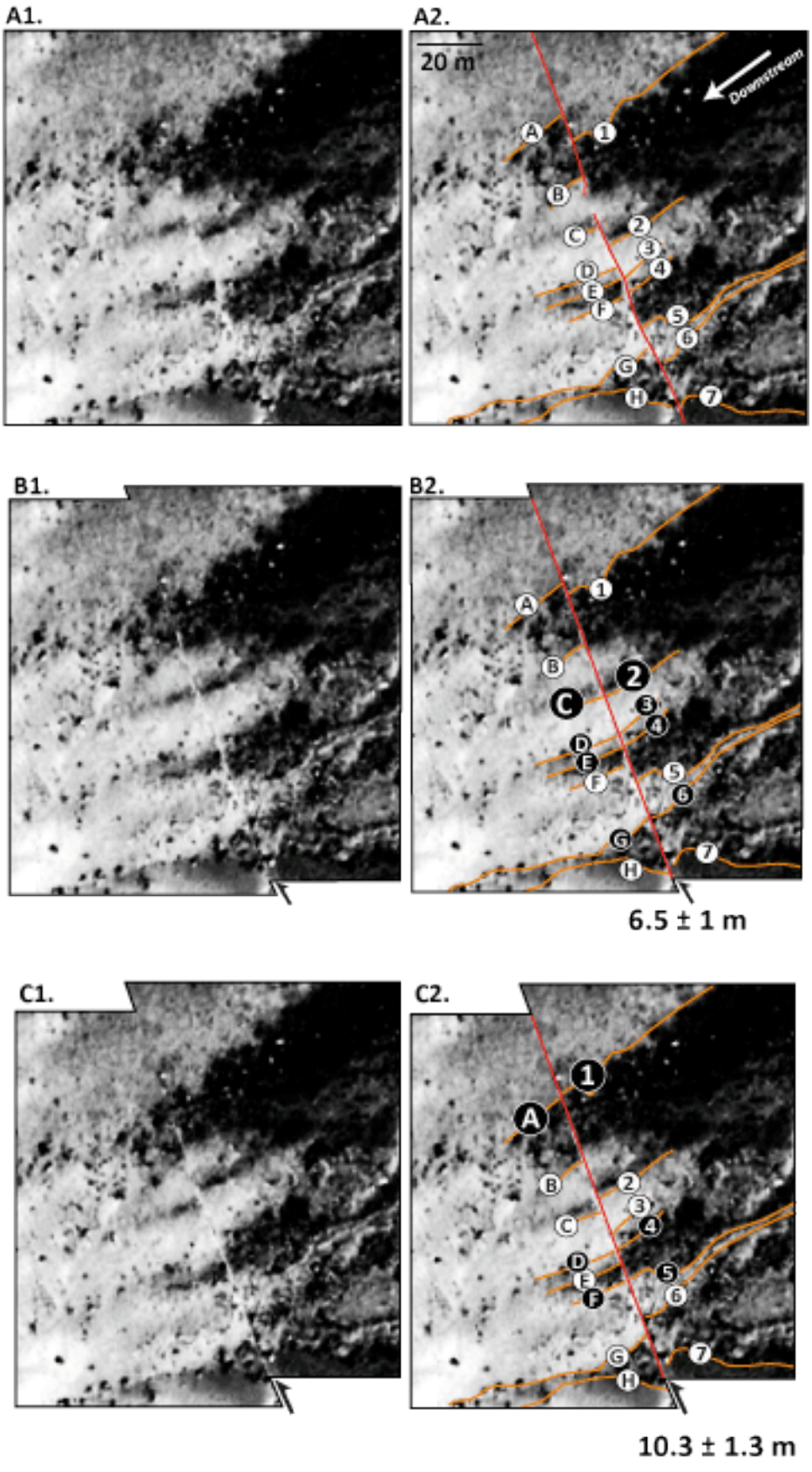

Characteristic Slip for 5 great earthquakes along the Fuyun fault in China. Klinger et al.

Figure Supp. 2b
klinger et al.

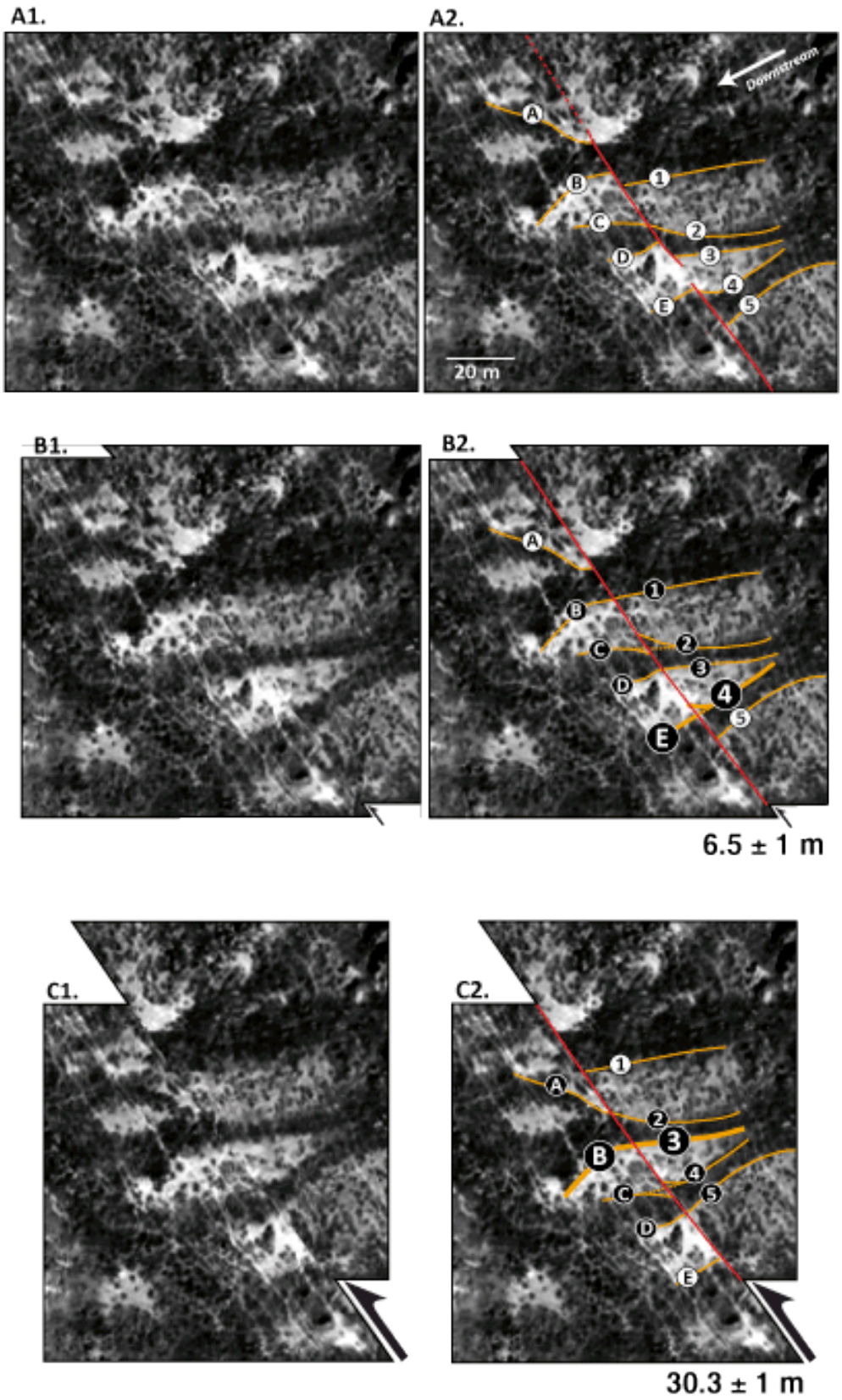

Characteristic Slip for 5 great earthquakes along the Fuyun fault in China. Klinger et al.

Figure Supp. 2c
klinger et al.

SITE D3

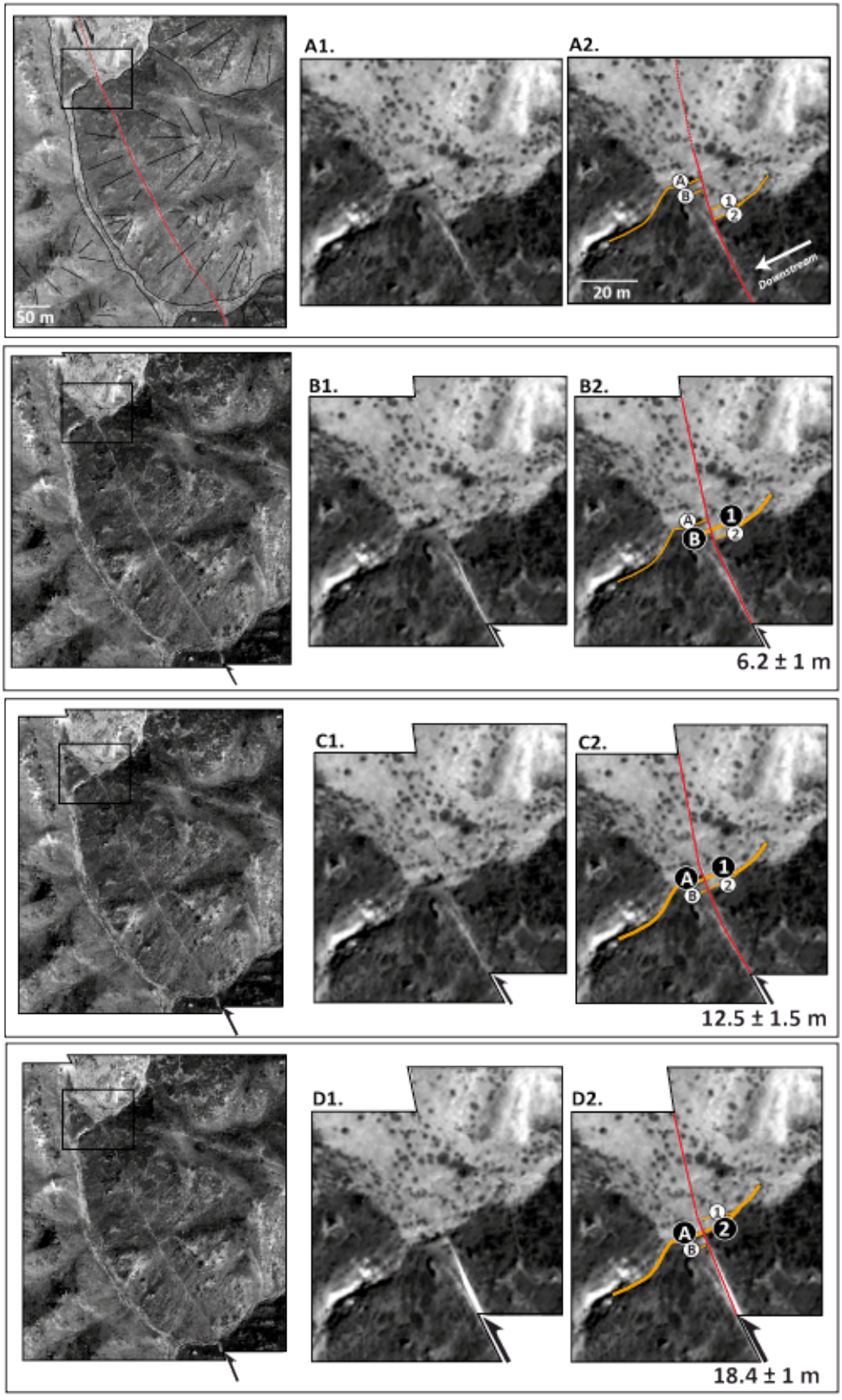

Figure Supp. 2d
klinger et al.

SITE D5

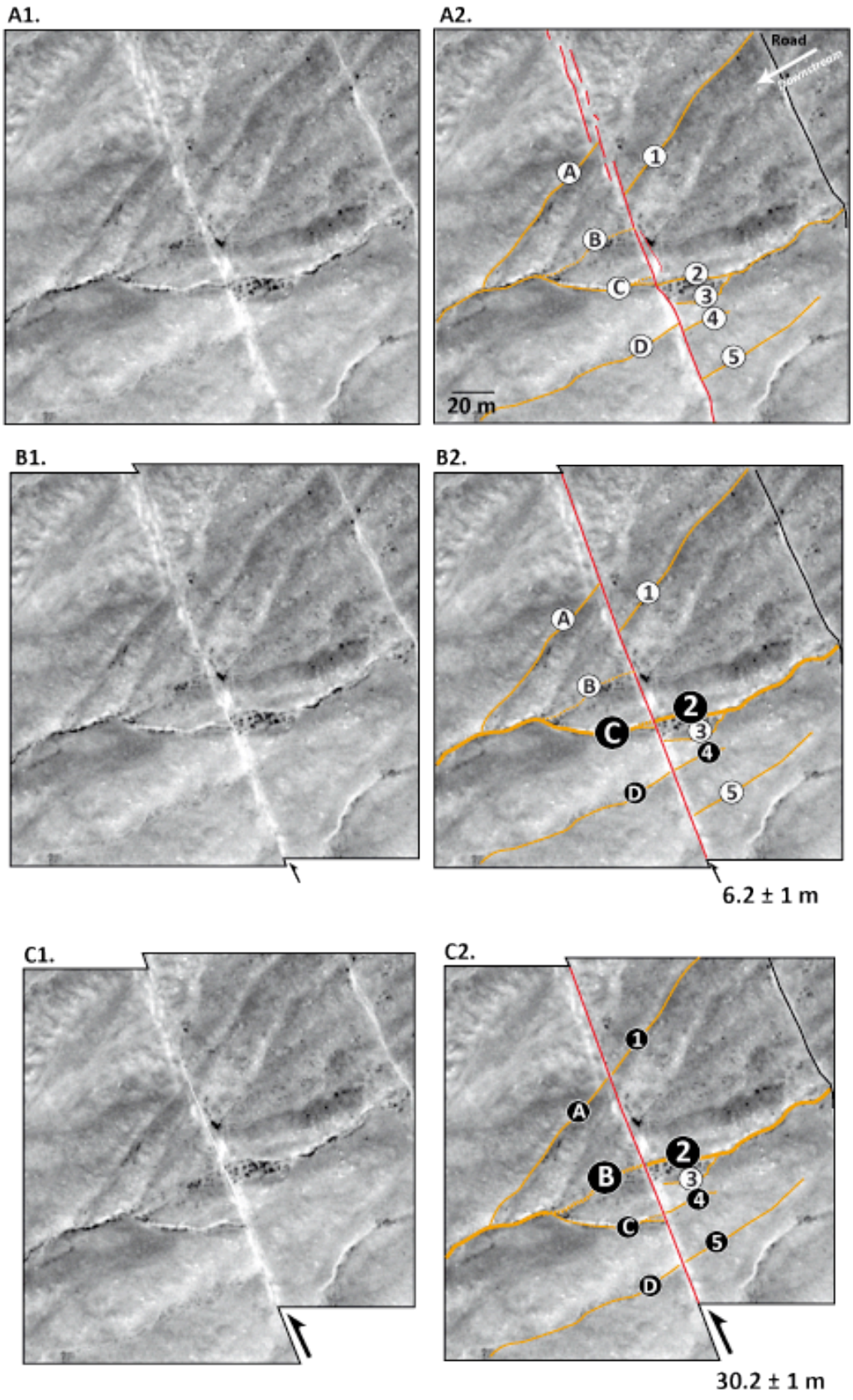

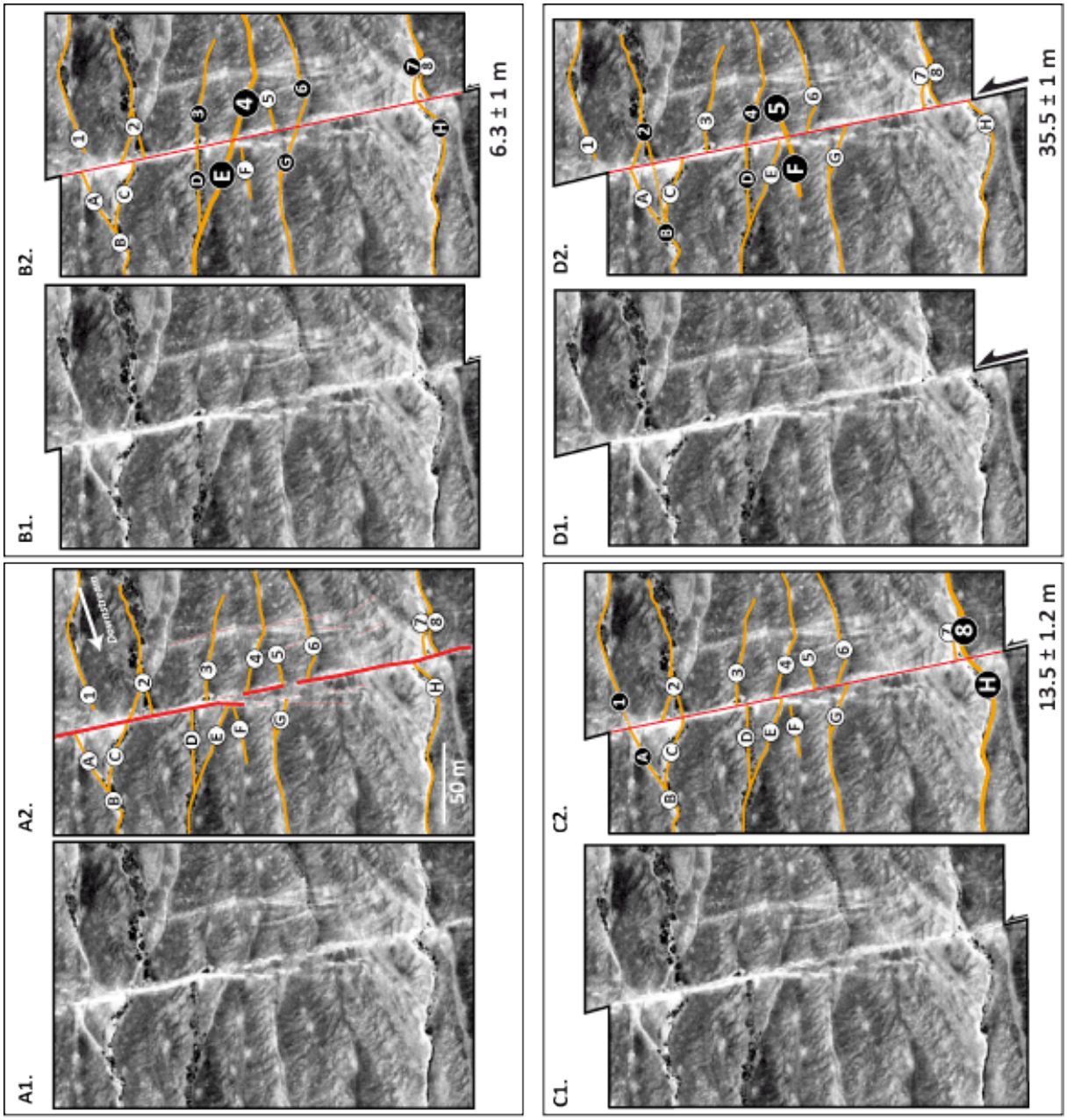

Figure Supp. 2e
Klinger et al.
SITE D6

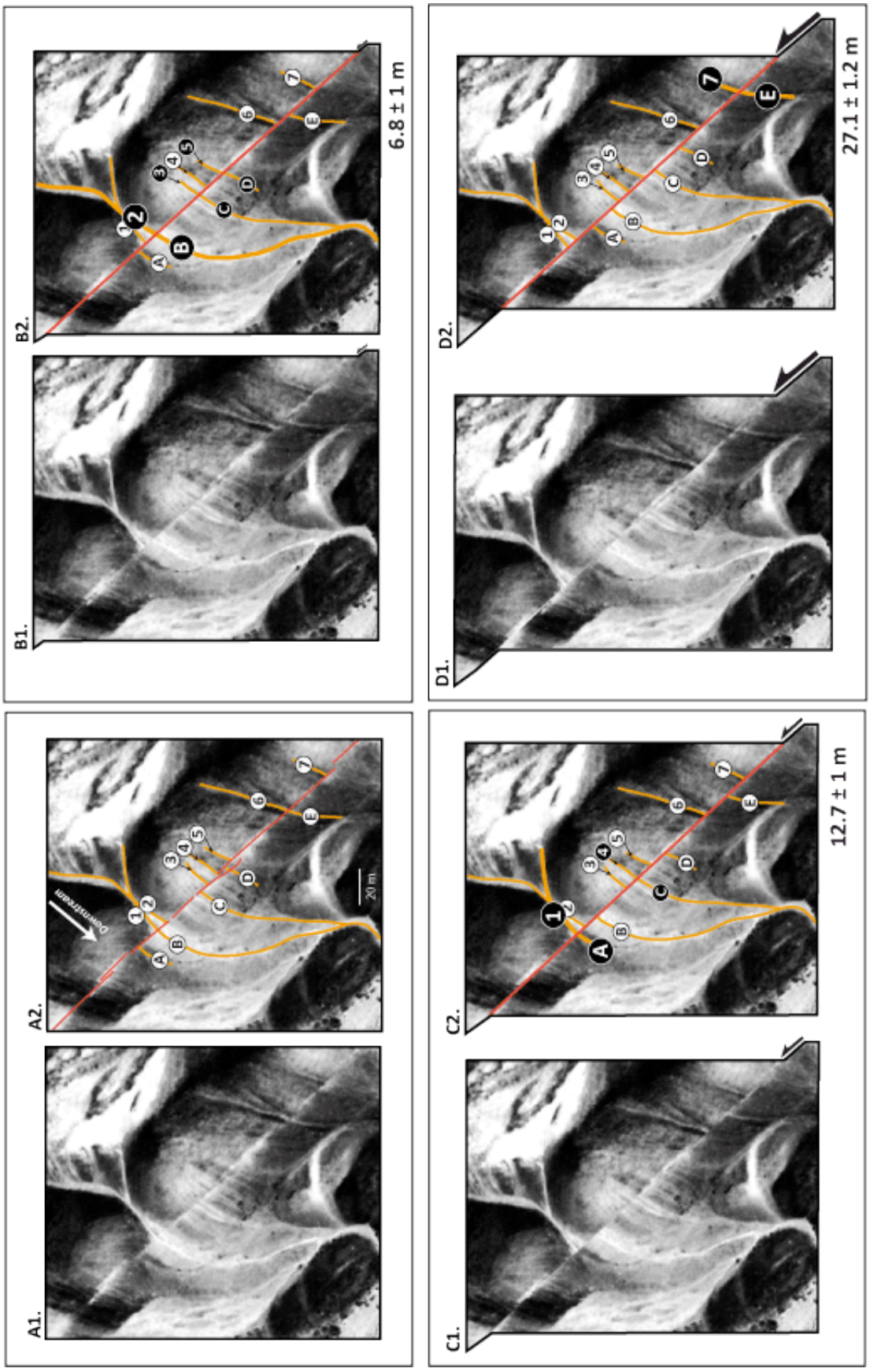

Figure Supp. 2f
klinger et al.
SITE D7

Characteristic Slip for 5 great earthquakes along the Fuyun fault in China. Klinger et al.

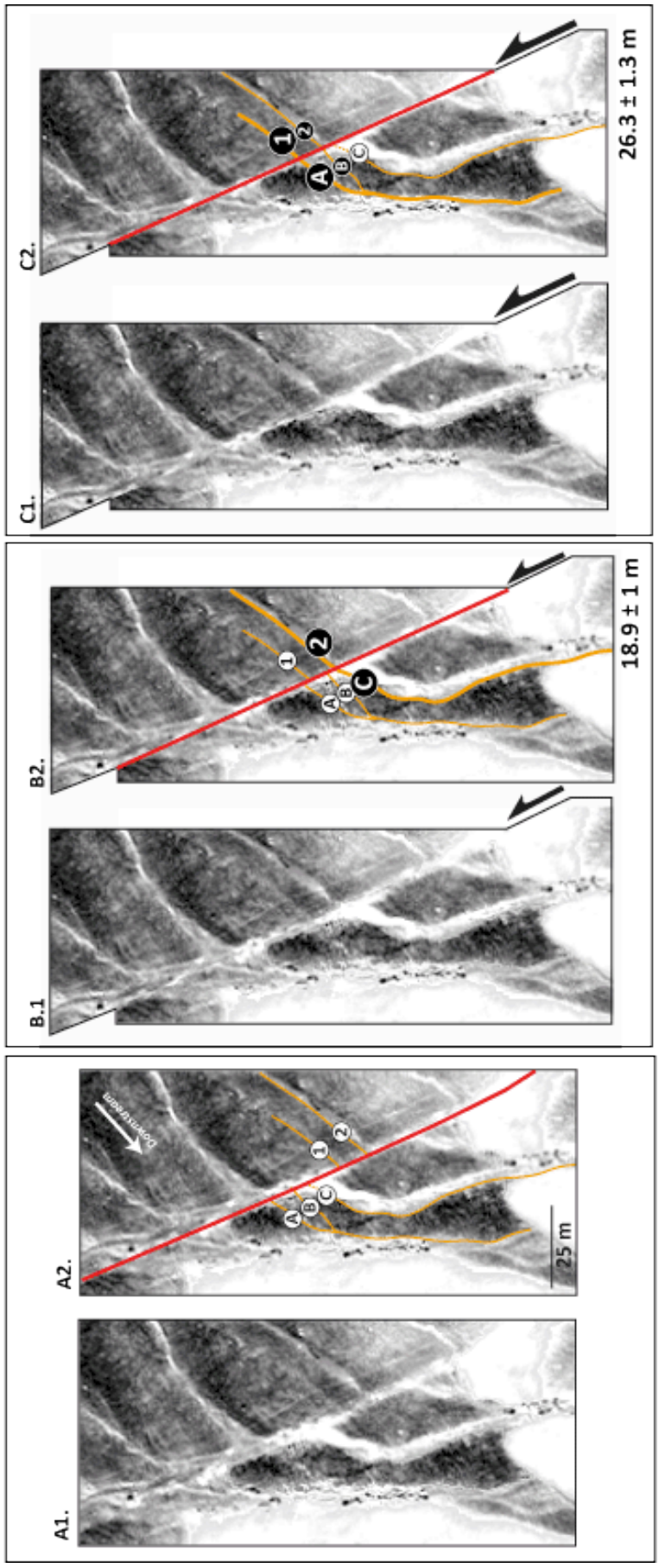

Figure Supp. 2g
klinger et al.

SITE D8

Characteristic Slip for 5 great earthquakes along the Fuyun fault in China. Klinger et al.

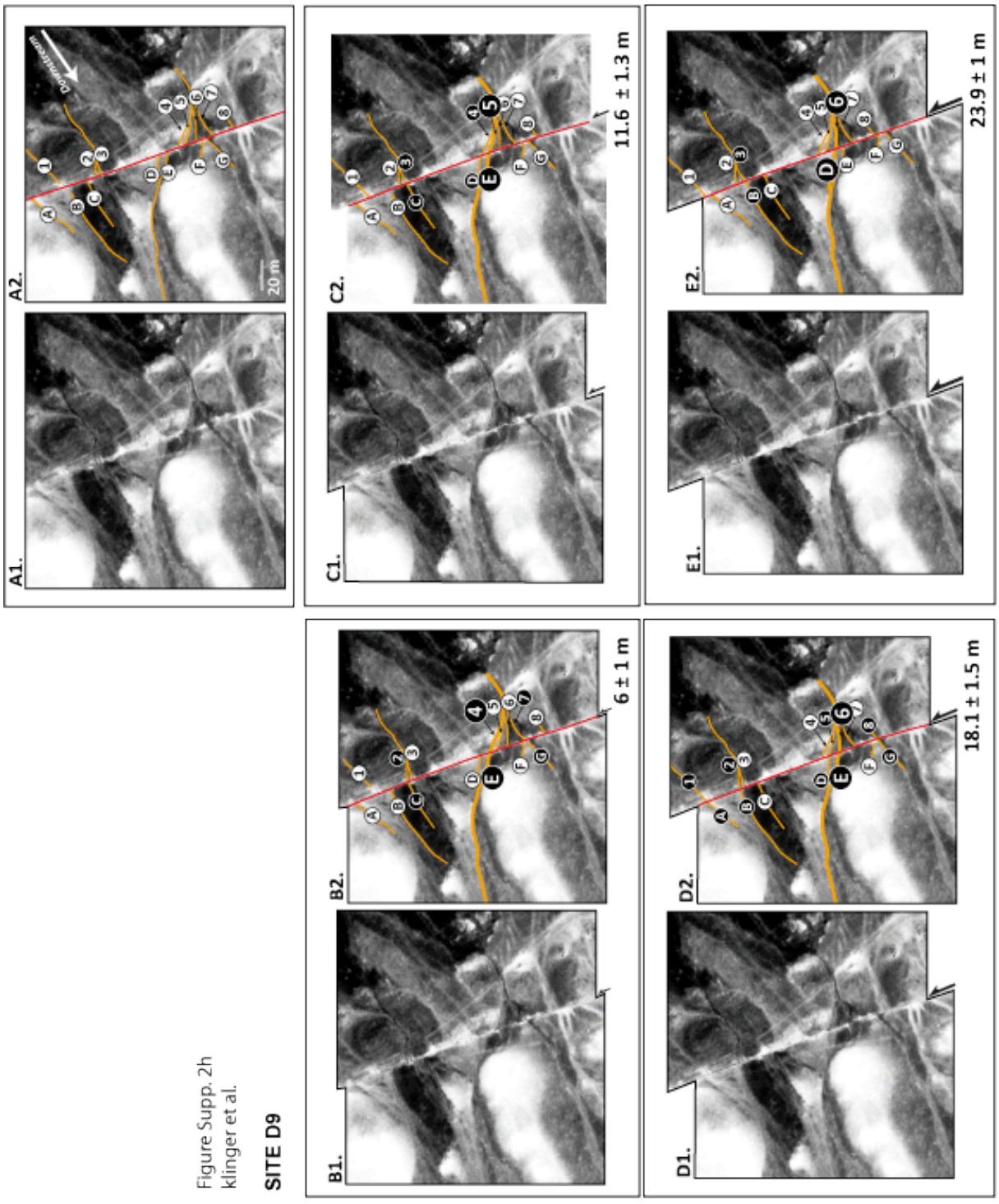

Figure Supp. 2h
klinger et al.

SITE D9

Figure Supp. 2i
klinger et al.

SITE D10

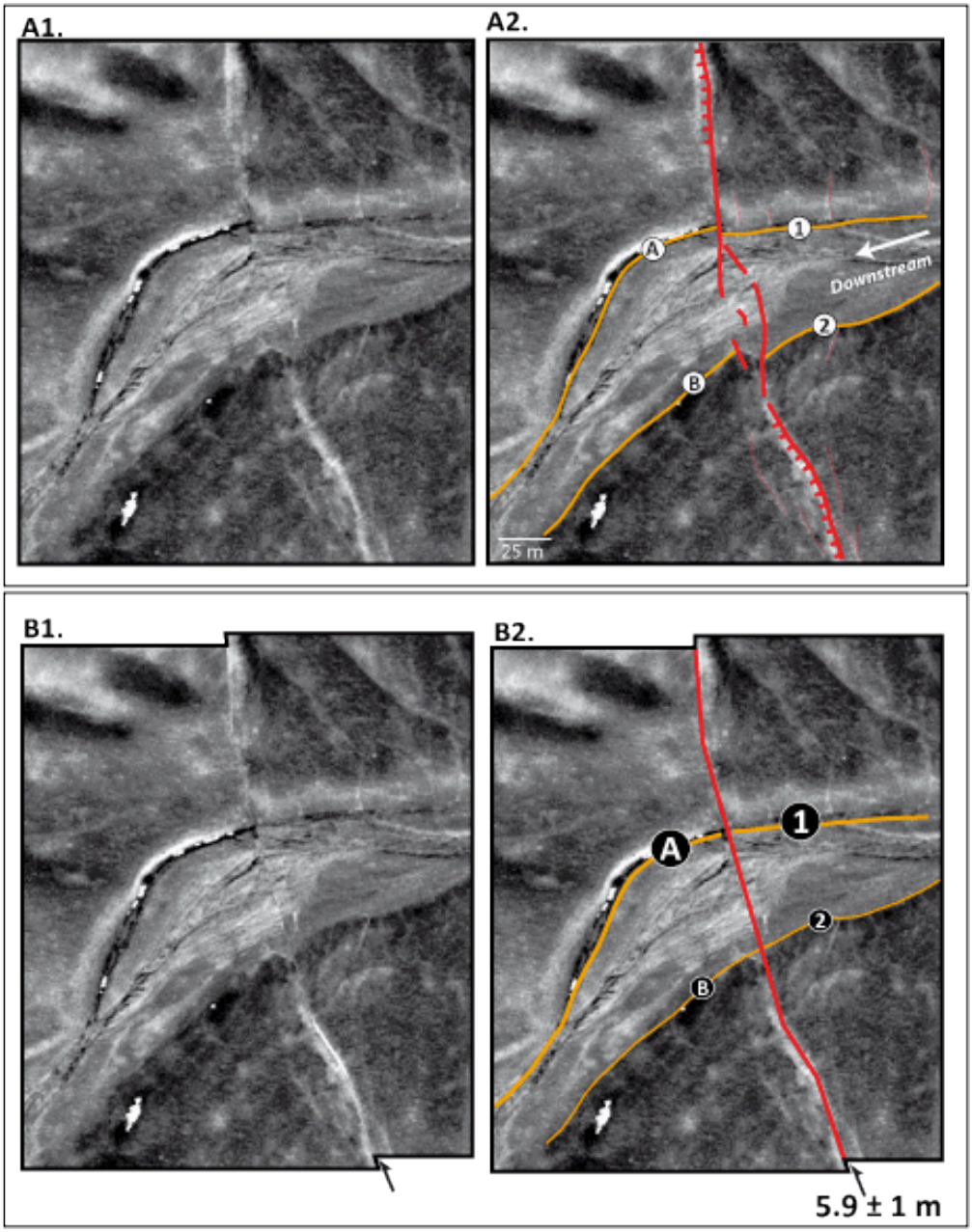

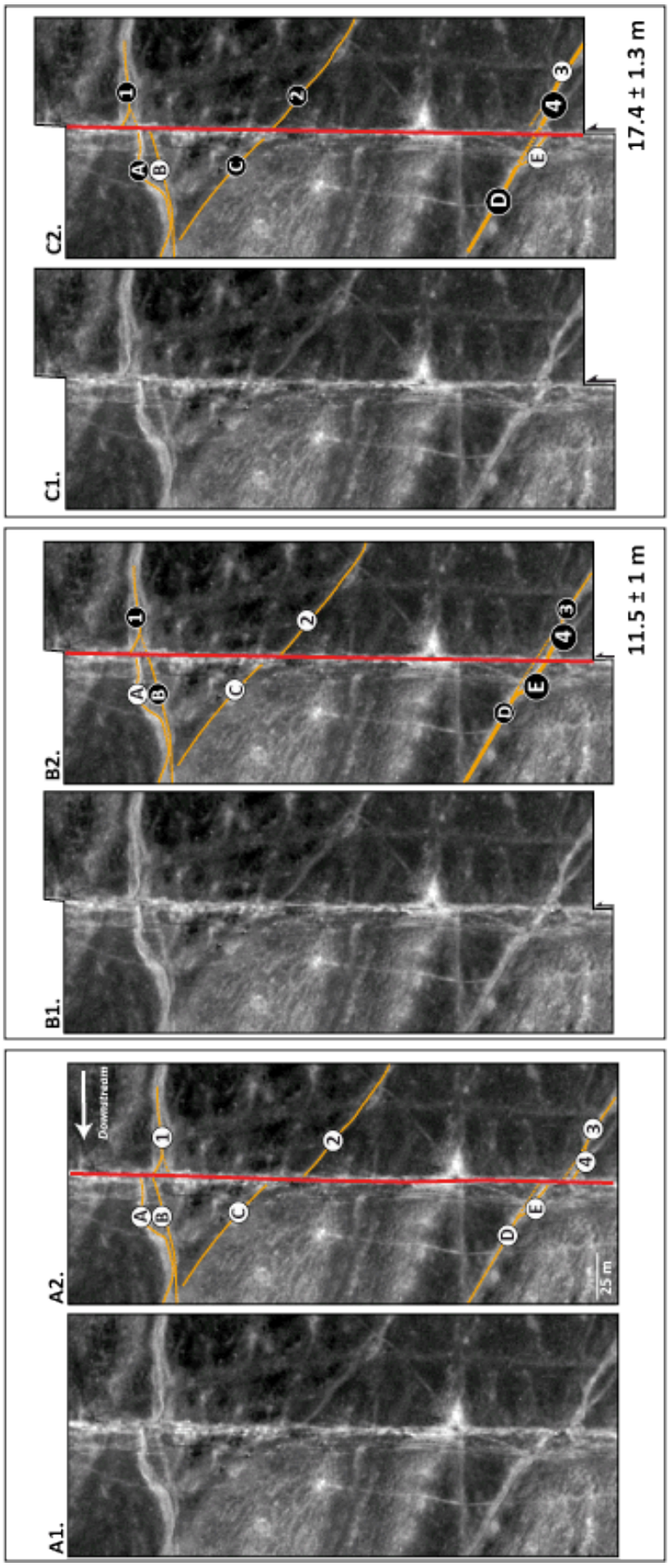

Figure Supp. 2j
klinger et al.
SITE D11

Characteristic Slip for 5 great earthquakes along the Fuyun fault in China. Klinger et al.

Figure Supp. 2k
klinger et al.

SITE D12

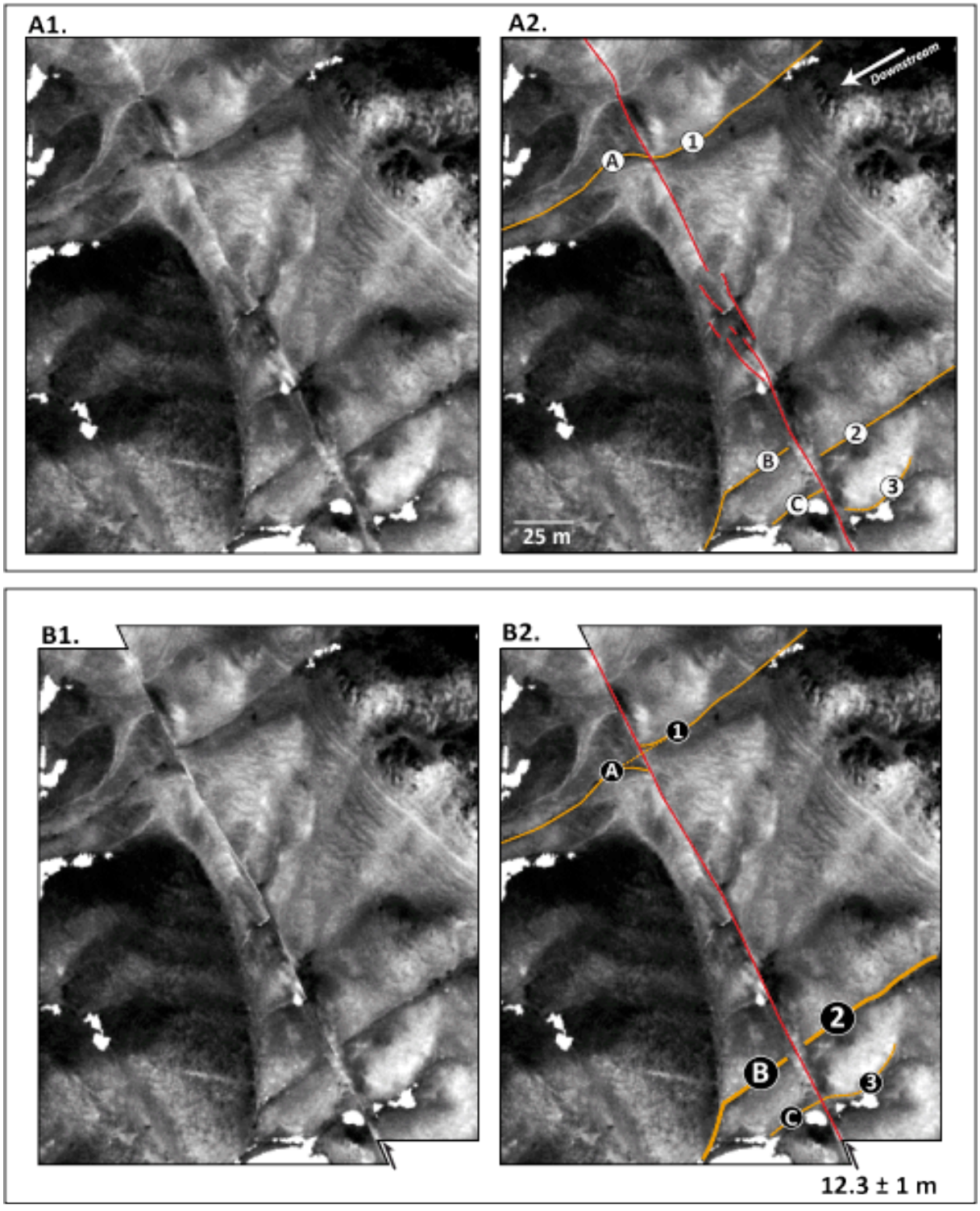

Characteristic Slip for 5 great earthquakes along the Fuyun fault in China. Klinger et al.

Figure Supp. 2l
klinger et al.

SITE D13

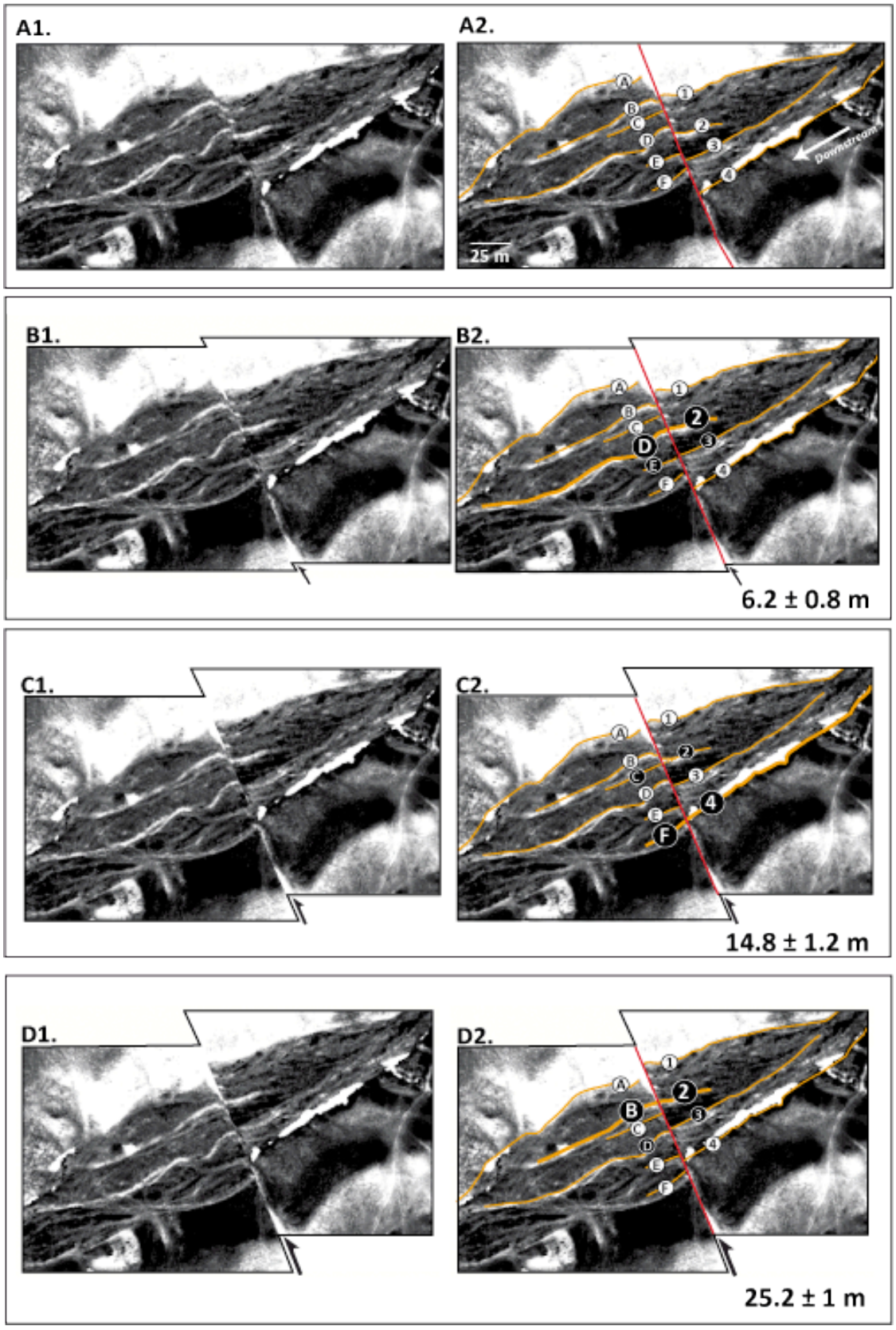

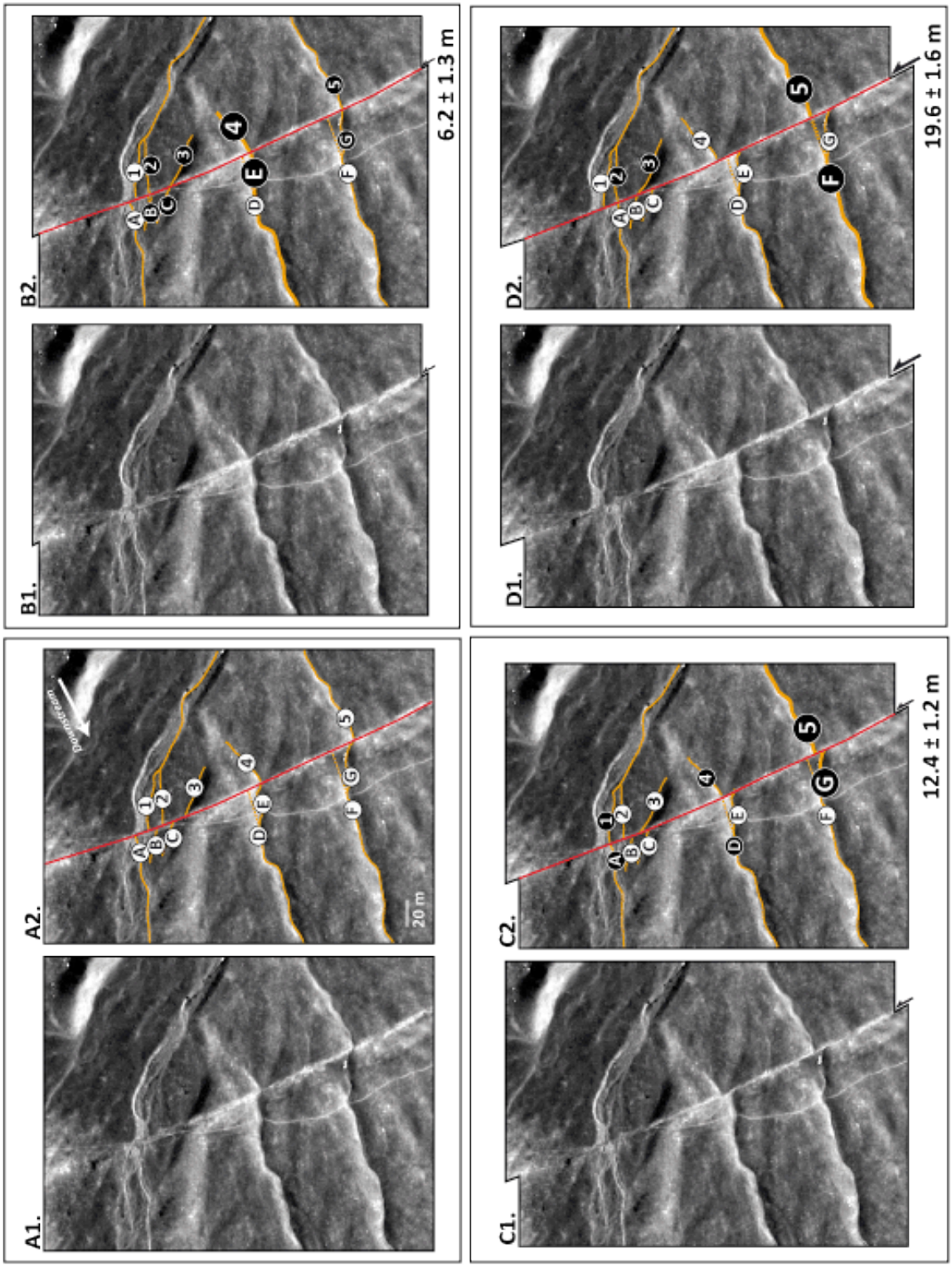

Figure Supp. 2m
klinger et al.
SITE D14

Figure Supp. 2n
klinger et al.

SITE D15

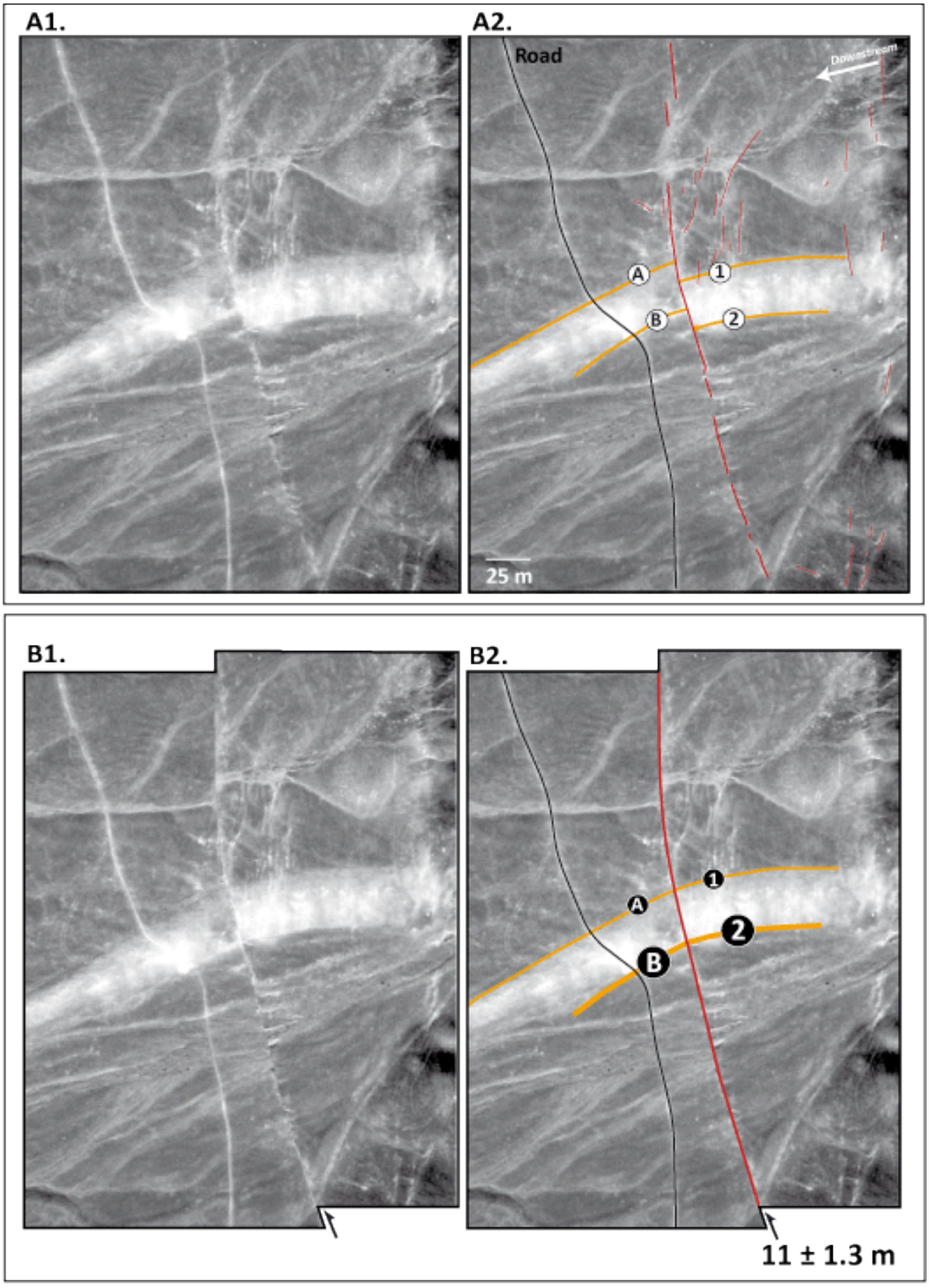

2/ **Comparison between field measurements and Quickbird offsets values**

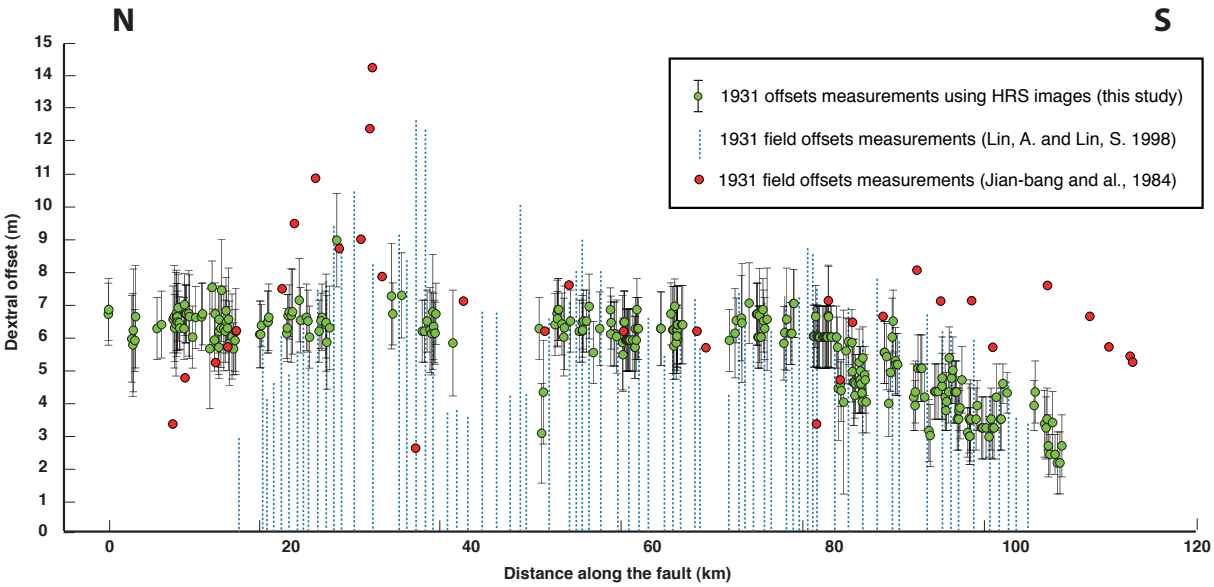

Figure 3: Comparison between 1931 co-seismic offset values collected in the field by Jianbang et al. (1984) and Lin and Lin (1998), and 1931 offset measurements from our image analysis. The datasets are in general agreement, but there are discrepancies at a few locations. Around km 35 for instance, Lin and Lin (1998) documented offsets larger than either to the north or south, while Jianbang et al. (1984) measured even larger offsets. Large vertical offsets have been reported along this section, which makes image analysis difficult. In fact, we failed to measure fresh horizontal offsets on the images at the same location. Similarly, at km 45, Lin and Lin (1998) observed 1931 offsets on order of 3 m where we could measure none on the images. This location might correspond to a segment boundary, where the rupture shows a high degree of complexity (main text fig. 1). South of km 80, our measurements are in a good agreement with the densest field observations of Lin and Lin (1998), while Jianbang et al's offsets (1984) are systematically larger. It is possible that the latter data reflects cumulative offsets.

Characteristic Slip for 5 great earthquakes along the Fuyun fault in China. Klinger et al.

3/ Methods

3.1/ Determination of characteristic slip amount

Analysis of the Quickbird offsets distribution from the entire dataset (fig. 4a) and northern 80 km subset (largest offsets, fig. 5a) shows well-separated peaks due to highly discontinuous slip accumulation with time. The sharpness of the peaks implies that individual earthquakes have a mean co-seismic slip larger than the slip variability along the fault. To a first order, the periodicity of the signal indicates that this mean slip is about the same for several seismic events. We use a discrete Fourier transform (DFT) to quantitatively characterize the frequency content of the offset distributions (fig. 4b and 5b). In practice, we construct an offset distribution histogram with bins centered every meter between 1 and 70m. Thus, we analyze a regular series of observations stacked along the entire rupture with a sampling length of 1 m. A characteristic wavelength $\Lambda \approx 6.2$ m emerges, which can be used as a mean value of the co-seismic slip along the Fuyun fault in the past. To verify that this characteristic value is compatible with the 1931 mean co-seismic slip, we select the smallest offset measurements along the fault (see main text fig. 1b) using a non-overlapping sliding window, with a width of 100 m, moving along the fault. For each window position we choose the smallest offsets. Then, we calculate the mean and standard deviation values of this subset of 290 offset measurements. We take the mean value, $lc = 6.3 \pm 1.2$ m, to represent the average co-seismic slip of the 1931 earthquake, excluding the northern normal fault section in this calculation. Both values (lc and Λ) are in agreement within error. Figure 4a and 5a show the peak-to peak distances calculated from the position of the modes obtained by linear interpolation of the cumulated distribution function. There is good agreement between the peak-to-peak distance, DFT's characteristic wavelength and the mean value of the 1931 offset. Such agreement between three independent estimates suggests that a repeating slip pattern for past earthquakes may be accurately predicted from the 1931 co-seismic slip distribution.

Characteristic Slip for 5 great earthquakes along the Fuyun fault in China. Klinger et al.

Figure 4a & 4b: Characteristic wavelength of offset measurement distribution along entire fault (110 km). a) Offset measurements stacked along entire fault. This offset distribution histogram is constructed with 1m-wide bins centered on integer of values between 1m and 70m. Peak to peak distances are calculated from the position of the modes obtained by linear interpolation of the cumulated distribution function. b) Discrete Fourier transform of offset measurement distribution. Position of first peak corresponds to a maximum wavelength Λ=6.24 m. Harmonics at $\Lambda/2$ and $\Lambda/3$ are indicated by dashed lines.

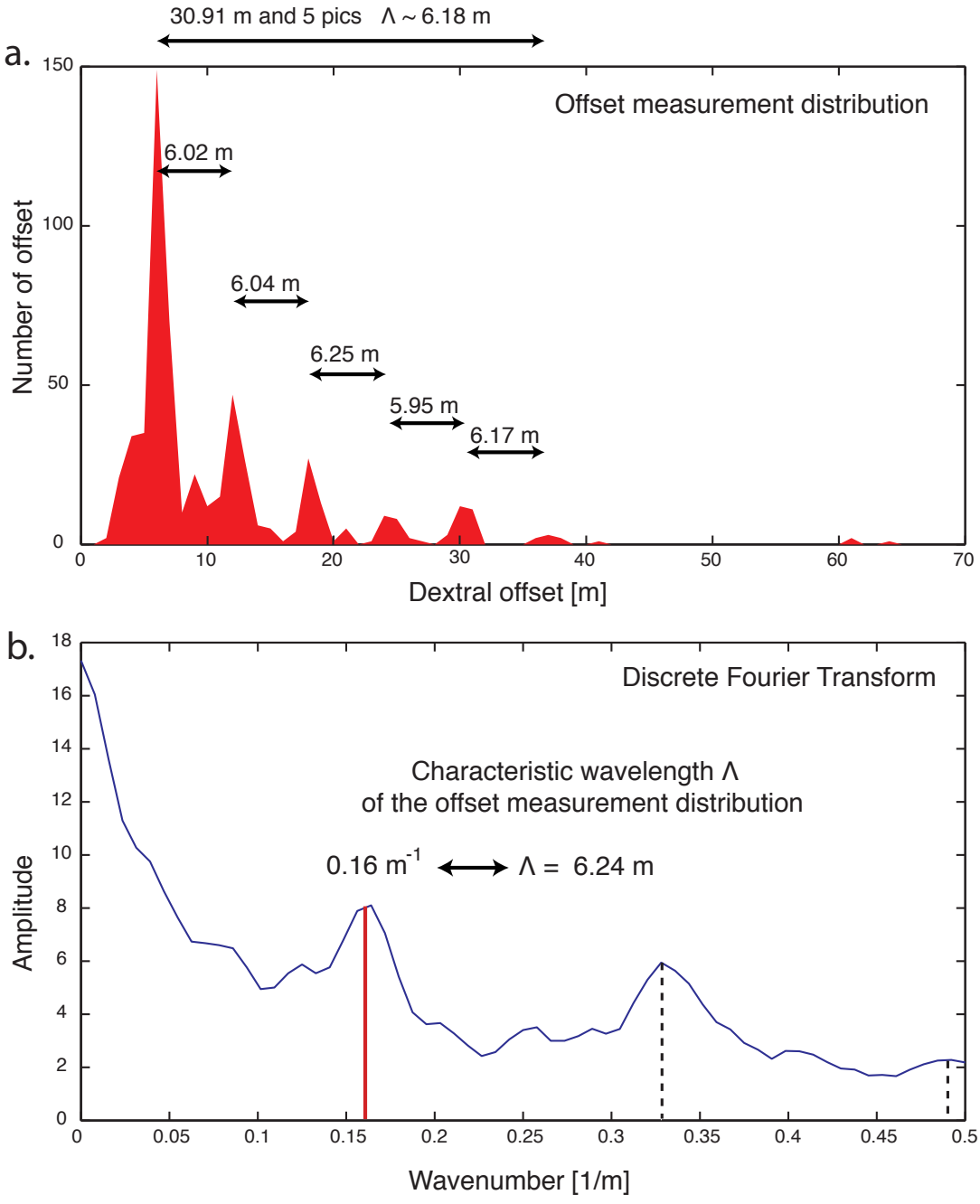

Figure 5a & 5b: Characteristic wavelength of offset measurement distribution along northern 80 km of rupture. a) Offset measurements stacked along northern 80k part of rupture. Histogram and peak to peak values obtained as in Fig. 4a. b) Discrete Fourier transform. Position of the first peak corresponds to a maximum wavelength Λ=6.09 m. Harmonics at Λ/2 and Λ/3 are indicated by dashed lines.

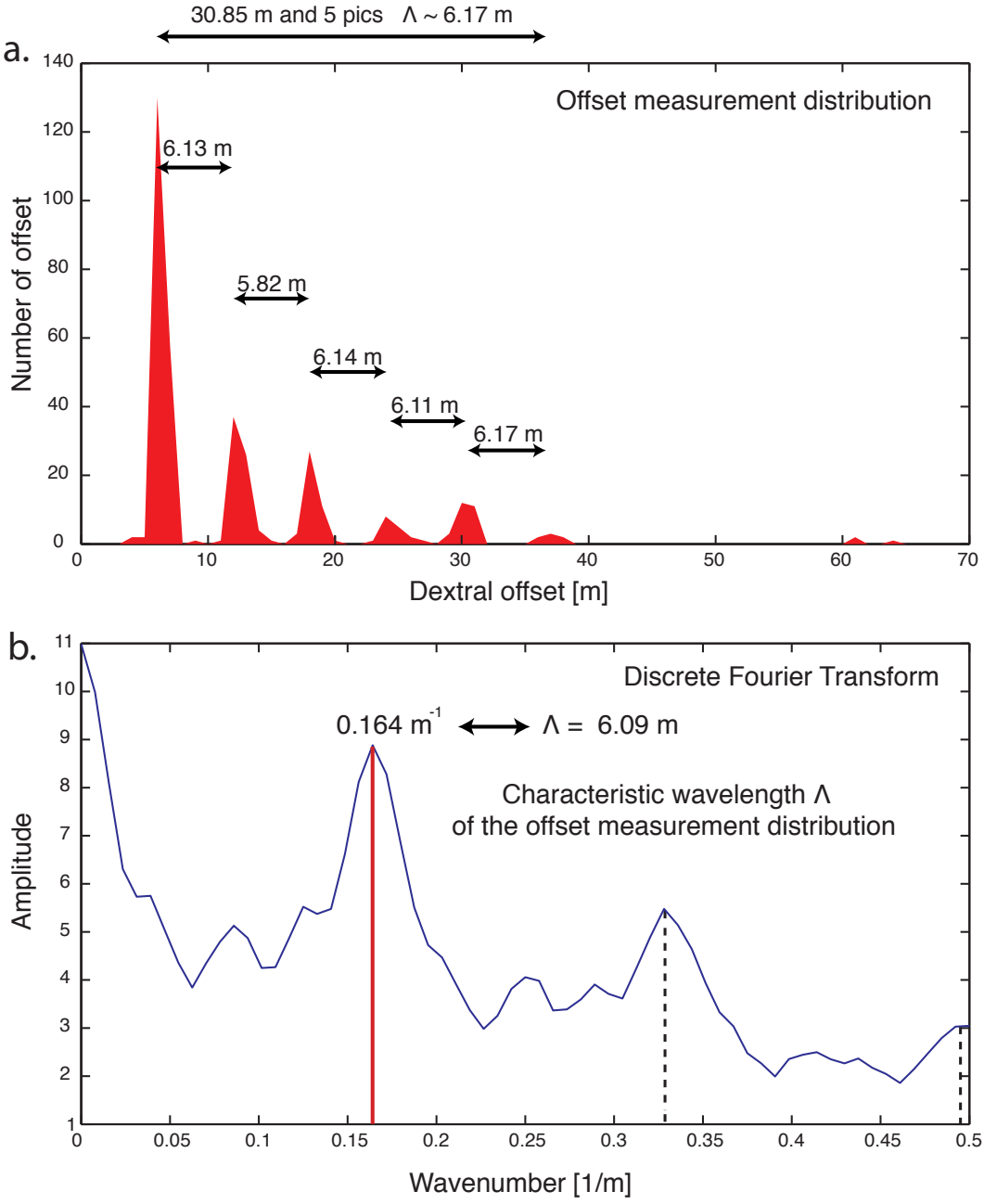

Characteristic Slip for 5 great earthquakes along the Fuyun fault in China. Klinger et al.

3.2/ Determination of geomorphic preservation constant

The shape and visibility of geomorphic markers degrade with time. Correspondingly, the Quickbird offset distribution shows a number of measurable markers that decreases with increasing cumulative slip (supplementary fig. 4a and 5b). The shape of this decay function may be used to define a constant characteristic of the geomorphic preservation in this region of Central Asia.

Clearly, trying to define the preservation of landforms with a single parameter is to oversimplify a complex natural process. In general, the evolution of stream channels and terrace risers involves a range of physical-chemical-biological-anthropological mechanisms that are individually difficult to quantify. Furthermore, while such processes may coexist in most environments, their relative influence is likely to vary from one area to another. Nevertheless, towards a first-order regional assessment, we use the Fuyun dataset to quantify landform degradation.

Assuming a characteristic slip model and a mean co-seismic slip of 6 m, offset measurements are distributed into classes corresponding to one, two, three earthquakes... using a non-overlapping sliding window of width ± 3m, moving by steps of 6m along the offset axis on main text fig. 1b. Fig. 6 shows, in log/normal coordinates, the probability density function (PDF) maxima (blue dots) of the offset measurements distribution, as a function of the number of characteristic earthquakes. The best fitting model (black line) is an exponential of the form

$$f_\lambda(n; \lambda) = \lambda \exp(-\lambda n) \quad (1)$$

where λ is a dimensionless constant characterizing the preservation of geomorphic markers. The exponential function likely reflects a stationary degradation process. For the whole 110 km-long rupture mapped, $\lambda = 0.55$. For only the northern 80km of the rupture, where offsets are best defined, $\lambda = 0.49$. λ is the logarithm of the ratio of the number of geomorphic markers for 2 successive earthquakes. For instance, considering the offset distribution in fig. 6a, the value $\lambda = 0.55$ indicates that the probability to observe a marker recording n events is 1.7 times greater than that to observe one recording (n+1) events.

Characteristic Slip for 5 great earthquakes along the Fuyun fault in China. Klinger et al.

To test the robustness of the model, we generate, through a Monte Carlo scheme, 5000 synthetic offset distributions, using the best-fitting constant $\lambda = 0.55$ (or $\lambda = 0.49$, for the northern rupture). Following the same procedure as for the field data, the PDFs of these synthetic distributions can be determined. Hence, error bars can be estimated, based on the mean and standard deviation (purple squares and bars in fig. 6). Despite one clear exception, the fit between data and synthetics is acceptable.

It is worth noting that the probability for a geomorphic marker to have recorded n events is given by

$$P(n) = \exp(-\lambda n)(1 - \exp(-\lambda)) \qquad (2)$$

The inference that the Fuyun fault generates characteristic earthquakes implies that λ is proportional to the earthquake recurrence time ΔT. Hence, the characteristic time for the preservation of geomorphic markers is

$$t_0 = \frac{\Delta T}{\lambda},$$

and the PDF for such preservation is of the form

$$f_t(t;t_0) = \frac{1}{t_0}\exp\left(\frac{-t}{t_0}\right). \qquad (3)$$

Note that such a relationship between preservation constant and recurrence time may be used to compare slip rates on two different faults in the same environment. Conversely, comparing measurements on two faults with characteristic behavior in different environments might provide useful insight into the factors that contribute to overall preservation.

Characteristic Slip for 5 great earthquakes along the Fuyun fault in China. Klinger et al.

Figure 6: Constant of preservation of geomorphic markers. (a) for entire fault and (b) for the northern 80 km of rupture with best preserved offsets. Blue dots are offset measurement PDFs plotted relative to number of characteristic earthquakes with best exponential fit shown as a purple line. PDFs of modeled data with associated error are purple diamonds and bars. See text for more detailed discussion.

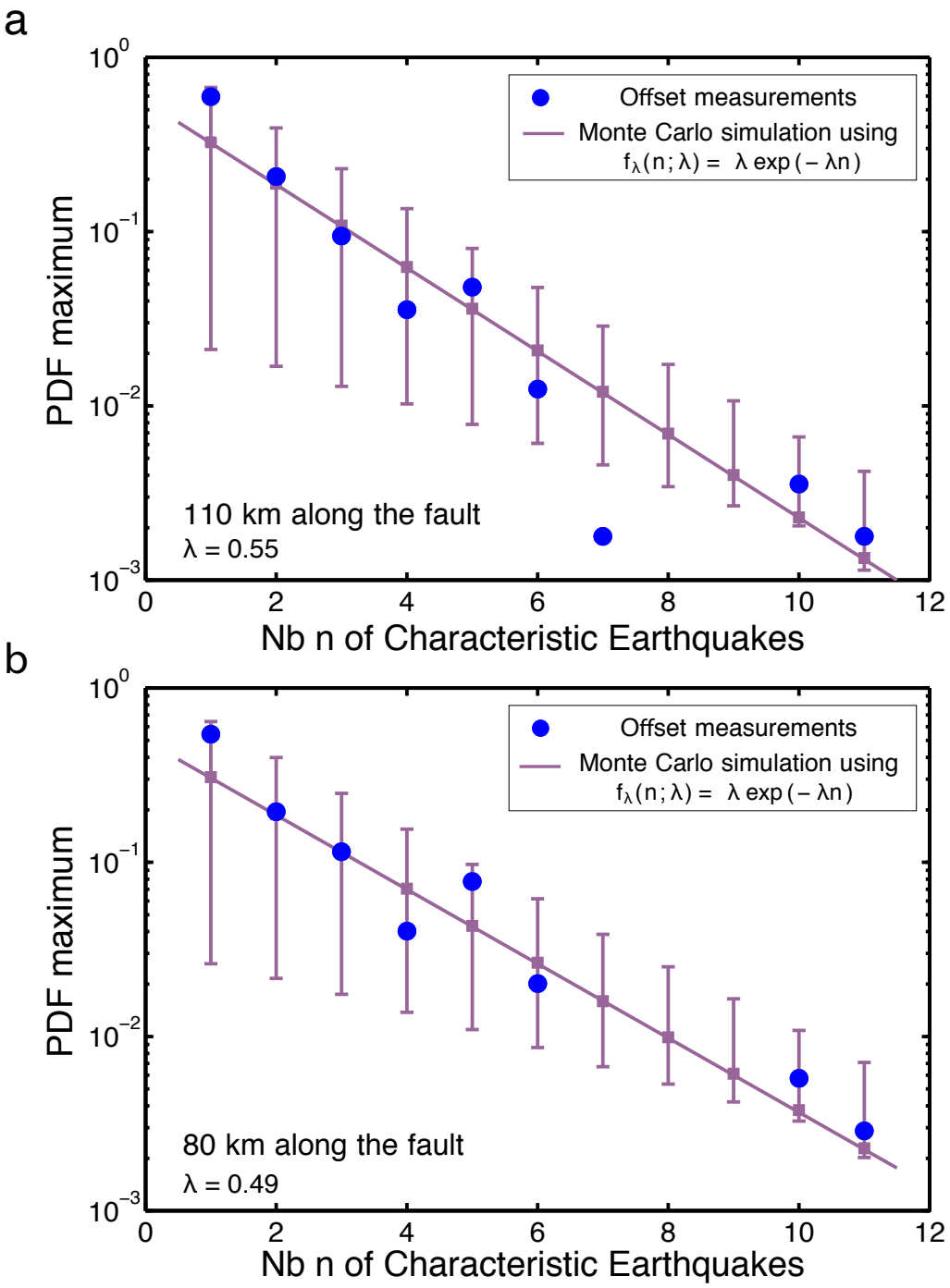

Characteristic Slip for 5 great earthquakes along the Fuyun fault in China. Klinger et al.

3.3/ Statistical modeling of offset measurements

We present here a synthetic stochastic model of multiple offsets along strike-slip faults generating characteristic earthquakes, such as the Fuyun fault. All model parameter values are determined from observations. The main goal is to verify that, with a minimal set of assumptions, one can satisfactorily reproduce the observed dataset and thus ensure that our interpretation of offset landforms is not biased by prejudice on what the offset distribution should be. We consider slip in all events to be statistically identical to coseismic slip in 1931, as characterized by the smallest offsets measured along the fault (see main text fig. 1). Using this data subset, we determine the mean and standard deviation (μ(x) and σ(x), respectively), of the co-seismic slip at each location x along the fault, obtained by cubic spline interpolation of the mean value and error associated with each measurement. We consider the local slip s(x) produced by a single event to be a random variable with a normal distribution

$$N\left(s(x);\mu(x),\sigma(x)\right) = \frac{1}{\sigma(x)\sqrt{2\pi}} \exp\left(-\frac{\left(s(x)-\mu(x)\right)^2}{2\sigma(x)}\right) \quad (4)$$

We also consider the number n of events recorded by a geomorphic marker to be a random variable with an exponential distribution $f_\lambda(n;\lambda)$, (see Eq. 1).

A large number of synthetic offset values is then generated using $f_\lambda(n;\lambda)$ and $N\left(s(x);\mu(x),\sigma(x)\right)$. Practically, three values are drawn at random to determine: 1/ The location x of the geomorphic marker along the fault. For simplicity, all locations are assumed to be equiprobable. 2/ The number of events (n) recorded by the geomorphic marker, sampled from the exponential distribution $f_\lambda(n;\lambda)$. 3/ The local cumulative slip produced by these n events, sampled from the normal distribution $N\left(s(x);\mu(x),\sigma(x)\right)$.

Thanks to the large number of synthetic data (10^6 simulations in main text fig. 3), probability densities to observe a given offset at a given location along the fault are obtained (main text fig. 3). For each offset at each location along the fault, the PDF of the number of events having produced the offset is also obtained. Accordingly, the symbols in main text fig.

3 show the most probable number of earthquakes seen by each geomorphic marker (mode of the probability distribution function).

4/

Caption for supplementary table 1:

Table 1 contains all the offset data presented in figure 1 of the main text. The best fitting, minimum and maximum acceptable values, measurement robustness index (see text for definition of this index) and location of each offset are listed.

Caption for supplementary table 2:

Table 2 presents the tabulated data from Jiangbang et al. (1984) and Lin and Lin (1998). Measurement locations, retrieved from published figures (no GPS or other precise positions are given in any of the two articles) should be considered approximate.

5/ References

Jianbang, S., S. Xianyue, and G. Shumo (1984), The Fuyun earthquake fault zone in Xinjiang, China, paper presented at International symposium on continental seismicity and earthquake prediction, Seismological Press, Beijing.

Klinger Y., Xu X., Tapponnier P., Van der Woerd J., Lasserre C., King, G. (2005), High-resolution satellite imagery mapping of the surface rupture and slip distribution of the Mw 7.8, 14 November 2001 Kokoxili earthquake, Kunlun fault, northern Tibet, China, Bull. Seis. Soc. Am., 95(5), 1970 - 1987.

Lienkaemper J. (2001), 1857 slip on the San Andreas fault southeast of Cholame, California, Bull. Seis. Soc. Am., 91(6), 1659 - 1672.

Lin, A., and S. Lin (1998), Tree damage and surface displacement: The 1931 M 8.0 Fuyun earthquake, J. Geol., 106, 751-757.

Xu, X., Hu G., Klinger Y., Tapponnier P., Van der Woerd J. (2006), Reevaluation of surface rupture parameters and faulting segmentation of the 2001 Kunlunshan earthquake (Mw7.8), northern Tibetan plateau, China, J. Geophys. Res., 111(B5), B05316, doi: 10.1029/2004JB003488.